Hui-Wang Cui*, Qun Fang and Guan-Ben Du

Structure of intercalated organic montmorillonite and its pyrolysis properties analyzed using the Agrawal integral equation

Abstract: We prepared intercalated organic montmorillonite (OMMT) from a pristine MMT and long-alkyl-chain quaternary ammonium salts (LACQAS). X-ray diffraction, Fourier transform infrared spectroscopy, scanning electron microscopy, and thermogravimetric analyses revealed that the amount, carbon atoms, and alkyl chains of LACQAS influenced the large value of $d_{(001)}$ of OMMT significantly. The $d_{(001)}$ stabilized at 100–150 mmol·(100 g)$^{-1}$ of LACQAS/MMT. The single LACQAS cations arranged in the form of a lateral layer or half-paraffin-type molecular structure between MMT layers, whereas the dual and triple LACQAS cations arranged in the form of a paraffin-type molecular structure. The pyrolysis temperature and maximum pyrolysis rate of OMMT increased greatly compared with those of MMT. The thermal weight loss of MMT was caused by the removed absorbed and structural water, whereas that of OMMT was by the pyrolysis of LACQAS. With the help of the Agrawal integral equation, the pyrolysis kinetics of MMT and OMMT were obtained using a trial-and-error method.

Keywords: intercalated nanocomposites; montmorillonite; pyrolysis; structure.

DOI 10.1515/secm-2012-0180
Received December 25, 2012; accepted September 27, 2014; previously published online December 22, 2014

***Corresponding author: Hui-Wang Cui,** Southwest Forestry University, Kunming 650224, Yunnan, China; College of Wood Science and Technology, Nanjing Forestry University, Nanjing 210037, Jiangsu, China; and Institute of Scientific and Industrial Research, Osaka University, Ibaraki 565-0047, Osaka, Japan, e-mail: cuihuiwang@hotmail.com
Qun Fang: School of Engineering, Zhejiang A&F University, Lin'an 311300, Zhejiang, China
Guan-Ben Du: Southwest Forestry University, Kunming 650224, Yunnan, China; and College of Wood Science and Technology, Nanjing Forestry University, Nanjing 210037, Jiangsu, China

1 Introduction

As a natural nanomineral, montmorillonite (MMT) is cheap and easily accessible. Its crystal structure is a 2:1-type layered silicate formed by an aluminum (or magnesium) octahedral layer inserted into two silicon oxygen tetrahedron layers. MMT has shown good expansion, dispersion, and absorption properties, and also can be made into mud, activated, organized, and modified easily. Moreover, the application fields of MMT have broadened greatly since the emergence of organic MMT (OMMT). Now, MMT and OMMT have been used in medicine and health, food, cosmetics, paint, printing ink, coating, building materials, metallurgy, petroleum well drilling, and other applications [1–10].

In our previous works, we obtained intercalated OMMT and applied it into the emulsion polymerization of polyvinyl acetate successfully [11–18]. In addition, we also used a polyhedral oligomeric silsesquioxane surfactant and Huisgen [2+3] cycloaddition (click chemistry) to exfoliate MMT into single layers and sheets of nanoparticles [19], and applied them into polybenzoxazine to improve the mechanical properties, thermal properties, and surface hydrophobicity [20, 21]. To continue expanding the application of MMT in polymers or polymeric composites and perform a systematic study on this topic, we prepared intercalated OMMT from a pristine MMT and different long-alkyl-chain quaternary ammonium salts (LACQAS). The preparation process was simplified without any ultrasonic dispersing, titrating, or vacuum drying. The structure and pyrolysis properties of the obtained OMMT were studied using X-ray diffraction (XRD), Fourier transform infrared spectroscopy (FTIR), scanning electron microscopy (SEM), and thermogravimetric analysis (TGA).

2 Materials and methods

2.1 Samples

Five hundred milliliters of water and 10 g of MMT were mixed together for 5 h with strong stirring. When the

mixture had become a suspension liquid, the temperature was increased to 70–80°C. A certain amount of LACQAS was dissolved in the mixture of water and hydrochloric acid, and then they were added into the suspension liquid and allowed to stand for 0.5–1 h. After strong stirring for 2–3 h, the colloid of OMMT was prepared. After washing, filtering, drying, and grinding, the solid, powdery OMMT composited with MMT (Zhejiang Fenghong New Material Co., LTD, Hangzhou, China) and different LACQAS was obtained. Here, LACQAS included dodecyl trimethyl ammonium bromide (DTAB), tetradecyl trimethyl ammonium bromide (TTAB), cetyl trimethyl ammonium bromide (CTAB), octadecyl trimethyl ammonium bromide (STAB), octadecyl trimethyl ammonium chloride (STAC), dioctadecyl dimethyl ammonium bromide (DOAB), and trioctadecyl methyl ammonium bromide (TOAB), all from Sigma-Aldrich (St. Louis, MO,USA).

2.2 Characterization

XRD data were collected using a DX-2000 wiggler beam line (Dandong Fangyuan, Dandong, China). A triangular bent Si (111) single crystal was employed to obtain a monochromated beam having a wavelength (λ) of 1.54184 Å. The value of $d_{(001)}$ was calculated using Bragg's law, $\lambda=2d\sin\theta$, where λ is the wavelength of the X-rays, d is the distance between two MMT layers, and θ is the diffraction angle. The FTIR spectra of the sample pellets were recorded using a NICOLET 380 FTIR spectrophotometer (Thermal Scientific, Waltham, MA, USA) and the conventional KBr disk method; 32 scans were collected at a spectral resolution of 1 cm^{-1}; the pellets used in this study were sufficiently thin to obey the Beer-Lambert law. SEM images were recorded using a Quanta 200 scanning electron microscope (FEI, Hillsboro, OR, USA) operated at an accelerating voltage of 200 kV. The thermal stabilities of the samples were measured using a TGA 92 thermogravimetric analyzer (SETARAM, Caluire, France) operated under a pure N_2 atmosphere. The sample (ca. 7 mg) was placed in a Pt cell and heated at a rate of 10°C·min^{-1} from 25°C to 750°C under a N_2 flow rate of 60 ml·min^{-1}. The thermal weight loss (C, %) was calculated as follows: $C=(m_i-m_f)/m_i\times100\%$, where m_i is the weight at onset temperature and m_f is the weight at offset temperature. The organic content (O, %) of samples was calculated with the formula $O=(m_1-m_2)/m_1\times100\%$, where m_1 is the weight of solid samples dried for 2 h at 120°C and m_2 is the weight of solid samples fired for 4 h at 400°C.

3 Results and discussion

3.1 Structure

As Table 1 shows, the $d_{(001)}$ increased with increasing STAB, suggesting the OMMT activated by STAB was an intercalated nanocomposite. Besides the temperature, stirring, time, etc., the intercalation is related closely to the cation exchange capacity (CEC) of MMT. The CEC is 90 mmol·(100 g)$^{-1}$ for the used MMT in this study. That is, 90 mmol of LACQAS can react completely with 100 g of MMT under ideal conditions, and their cations can intercalate into MMT layers fully without any being wasted or becoming residue. However, this cannot be achieved in a real study; thus, increasing the amount of LACQAS to improve the intercalation is always conducted. When STAB was <90 mmol·(100 g)$^{-1}$ of MMT, the cations exchanged strongly with the metal cations (K^+, Na^+, Ca^{2+}, Mg^{2+}, Fe^{2+}, etc.) between MMT layers. As Table 1 shows, the $d_{(001)}$ increased from 1.263 to 1.912 nm in the range of 0–90 mmol·(100 g)$^{-1}$ of STAB/MMT. The increment of $d_{(001)}$ was small because the MMT layers were distracted to a limited extent owing to the limited amount of STAB. This case was changed totally when STAB was ≥90 mmol·(100 g)$^{-1}$ of MMT because of the

Table 1 MMT layers influenced by the amount of STAB.

STAB/MMT [mmol·(100 g)$^{-1}$]	θ (°)	$d_{(001)}$ (nm)	d_0 (nm)	α (°)	STAB/MMT [mmol·(100 g)$^{-1}$]	θ (°)	$d_{(001)}$ (nm)	d_0 (nm)	α (°)
0	3.50	1.263	0.303	–	130	2.13	2.074	1.114	24.11–25.09
50	3.11	1.421	0.461	9.73–10.11	140	2.11	2.094	1.134	24.57–25.57
60	2.92	1.513	0.553	11.70–12.15	150	2.09	2.114	1.154	25.04–26.06
70	2.70	1.636	0.676	14.35–14.91	160	2.11	2.094	1.134	24.57–25.57
80	2.48	1.782	0.822	17.54–18.23	170	2.12	2.084	1.124	24.34–25.33
90	2.31	1.912	0.952	20.43–21.25	180	2.14	2.065	1.105	23.90–24.87
100	2.13	2.074	1.114	24.11–25.09	190	2.15	2.055	1.095	23.67–24.63
110	2.15	2.055	1.095	23.67–24.63	200	2.15	2.055	1.095	23.67–24.63
120	2.14	2.065	1.105	23.90–24.87					

sufficient amount of STAB and the strong exchange capability of cations. The cations filled into the gaps and were absorbed to the skeletons of the MMT layers. They even exchanged with the Fe^{3+}, Al^{3+}, and Si^{4+} cations that were hardly substituted. As Table 1 shows, the $d_{(001)}$ changed from 2.055 to 2.114 nm in the range of 100–150 mmol·(100 g)$^{-1}$ of STAB/MMT. Therefore, MMT layers were distracted greatly and fully; the $d_{(001)}$ of OMMT increased significantly and stabilized at 100–150 mmol·(100 g)$^{-1}$ of MMT. If the amount of STAB continued to increase, the $d_{(001)}$ changed slightly. In the range of 160–200 mmol·(100 g)$^{-1}$ of STAB/MMT, the $d_{(001)}$ varied between 2.055 and 2.094 nm (Table 1), which were not larger than those in the range of 100–150 mmol·(100 g)$^{-1}$ of STAB/MMT. This is because STAB cations had exchanged with the metal cations in the MMT layers almost completely, and the excess or surplus STAB cations made use of every bit of space between the layers and became overlaid and stacked together. Therefore, the amount of STAB was preferably up to 100–150 mmol·(100 g)$^{-1}$ of MMT in this study.

On the basis of the above description, the amount of 150 mmol·(100 g)$^{-1}$ of LACQAS/MMT was used in this study, and the OMMT was prepared from pristine MMT and different LACQAS. As Table 2 shows, the $d_{(001)}$ increased significantly. The OMMT activated by different LACQAS, including DTAB, TTAB, CTAB, STAB, STAC, DOAB, and TOAB, all were intercalated nanocomposites. The longer the alkyl chain, the greater the $d_{(001)}$. The $d_{(001)}$ increased as the alkyl chain length of LACQAS increased. As the alkyl chain length increased from DTAB to TTAB, CTAB, and STAB, the $d_{(001)}$ showed increasing values at 1.819, 1.833, 1.973, and 2.114 nm, respectively (Table 2). LACQAS are cationic surfactants. Besides the physical absorption and distribution, the absorption caused by exchangeable ions also often occurred as follows: Me-MMT+CH_3-$(CH_2)_m$NX→MeX+$CH_3(CH_2)_m$N-MMT, where Me is the metal cation, X is the halogen substituent, and m is the number of carbon atoms. The $d_{(001)}$ of OMMT activated by STAB and STAC were 2.114 and 2.094 nm, respectively, at 150 mmol·(100 g)$^{-1}$ of MMT, showing that the halogen substituent did not have any great effect on the layers.

Table 2 MMT layers influenced by different LACQAS.

LACQAS	θ (°)	$d_{(001)}$ (nm)	d_0 (nm)	L_C (nm)	L (nm)	α (°)
MMT	3.50	1.263	0.303	–	–	–
DTAB	2.43	1.819	0.859	1.668	1.868–1.968	25.88–27.38
TTAB	2.41	1.833	0.873	1.921	2.121–2.221	23.15–24.31
CTAB	2.24	1.973	1.013	2.174	2.374–2.474	24.17–25.26
STAB	2.09	2.114	1.154	2.427	2.627–2.727	25.04–26.06
STAC	2.11	2.094	1.134	2.427	2.627–2.727	24.57–25.57
DOAB	1.11	3.980	3.020	4.704	4.704	39.95
TOAB	1.08	4.090	3.130	4.704	4.704	41.71

$d_{(001)}$ is related closely to the arrangement of LACQAS cations between MMT layers. In the low-charge dense layered silicates, the LACQAS cations with short alkyl chains arrange in the form of a lateral layer and those with long alkyl chains in the form of dual lateral layers; in the high-charge dense layered silicates, the LACQAS cations arrange in the form of a paraffin-type molecular structure, a dual-paraffin-type molecular structure, and fake triple layers, etc. (Figure 1) [22–25]. LACQAS cations are absorbed between or onto MMT layers. For a cation, the end with positive charge points to the absorbed layer and the non-polar end deviates from the layer. The cation arranges between MMT layers and forms an intersection angle through this physical absorption effect. The relationship among the $d_{(001)}$, α, and L is $d_{(001)}=L\sin\alpha+0.96$ [26], where α is the intersection angle of a LACQAS cation to the layer and L is the length of a LACQAS cation.

$d_{(001)}$ is made up of d_0 and 0.96 nm that follows $d_{(001)}=d_0+0.96$, where d_0 is the actual distance between two MMT layers and 0.96 nm is the thickness of a single MMT layer. The d_0 increased as $d_{(001)}$ increased (Tables 1 and 2). The length of an alkyl chain (L_C) is calculated by the Tanford equation, $L_C=0.15+0.1265m$ [27], where m is the carbon atom number in an alkyl chain. The length of a LACQAS cation (L) can be calculated by $L=L_C+L_G$, where L_G is the length of an ammonium ion in a LACQAS cation at 0.20–0.30 nm.

The arrangement of LACQAS cations between MMT layers is also related to the configuration of the nitrogen atom. As Figure 2 shows, the configuration is a tetrahedron connected by alkyl chains or methyl at four vertexes. If the connected alkyl chains increase from 1 to 2, even to 3, the flexibility of the configuration decreases whereas the upright stability increases. Because of this specific configuration and the bond angles of tetrahedron, the MMT layers were distracted and stretched. As Table 2 shows, the $d_{(001)}$ was 2.114, 3.980, and 4.090 nm for OMMT activated by STAB, DOAB, and TOAB, respectively. The increment of $d_{(001)}$ was 1.886 nm as the alkyl chains of LACQAS cations increase from 1 (STAB) to 2 (DOAB), but only 0.110 nm from 2 (DOAB) to 3 (TOAB). The arrangement of LACQAS cations between MMT layers was determined by d_0, L_C, L_G, L, and α. DTAB, TTAB, CTAB, STAC, and STAB with single LACQAS cations arranged in the form of a lateral layer and a half-paraffin-type molecular structure, whereas DOAB and TOAB with dual and triple LACQAS cations arranged in the form of a paraffin-type molecular structure.

Figure 3 shows the FTIR spectra of STAB, DOAB, TOAB, MMT, and OMMT. The transmittance peaks near

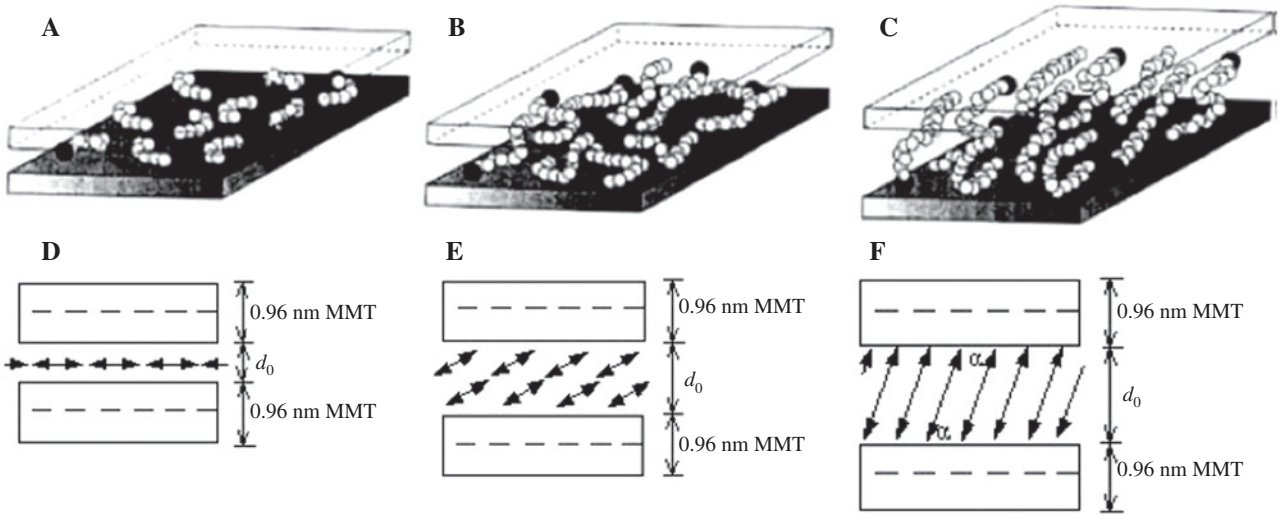

Figure 1 Arrangement of LACQAS cations in MMT layers.
(A) Short alkyl chain, (B) intermediate alkyl chain, (C) long alkyl chain, (D) lateral layer, (E) half-paraffin-type molecular structure, and (F) paraffin-type molecular structure, where d_0 is the actual distance between two MMT layers and 0.96 nm is the thickness of an MMT layer.

3600–3370 cm^{-1} and 1640 cm^{-1} for the stretching vibration and bending vibration of -O-H in MMT and OMMT represented the absorbed water between layers and the crystal water in crystal lattices. The dual transmittance peaks near 2920–2840 cm^{-1} for the symmetrical and asymmetrical stretching vibration of -C-H in $-CH_3$ and $-CH_2-$, the transmittance peaks near 1470–1480 cm^{-1} for the asymmetrical deformation vibration of -C-H in $-C-CH_3$ and deformation vibration of -C-H in $-CH_2$, and the transmittance peaks near 720 cm^{-1} for the rocking vibration of -C-H in $-(CH_2)_z$ ($z \geq 4$) combined together to show the entrance of LACQAS cations into the MMT layers. In the fingerprint region <1333 cm^{-1}, the FTIR spectra of MMT and OMMT were almost the same. They all displayed the characteristic transmittance peaks of MMT, such as asymmetrical stretching vibration of Si-O-Si near 1010 cm^{-1}, stretching vibration of Al-O-H near 920 cm^{-1}, stretching vibration of Fe-O-H near 890 cm^{-1}, stretching vibration of Mg-O-H near 790 cm^{-1}, etc., showing that the layered silicate skeleton did not change after the LACQAS cations exchanged with the metal cations between MMT layers. It can be seen that the skeletons of MMT and OMMT were similar, but not the same. In addition, no chemical bond was found from the FTIR spectra, but only physical absorptions between MMT and LACQAS. The transmittance bands of MMT and LACQAS stacked with those of OMMT. Neither new transmittance bands formed, nor did existing transmittance bands disappear.

As Figure 4 shows, OMMT presented a different surface morphology compared with that of MMT. MMT was a regular, clustered, compact solid with crystal characteristics; the surface was structured, flat, smooth, and with no crimping (Figure 4A). The surface of OMMT was changed totally after the intercalation of LACQAS. The OMMT

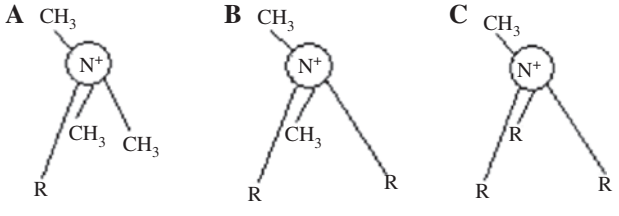

Figure 2 Configuration of the nitrogen atom in LACQAS.
(A) Single alkyl chain, (B) dual alkyl chains, and (C) triple alkyl chains, where R=alkyl chain.

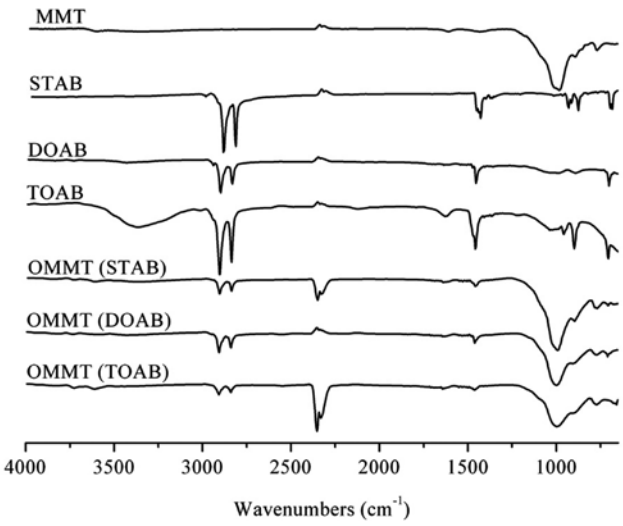

Figure 3 FTIR spectra of MMT, STAB, DOAB, TOAB, and OMMT.

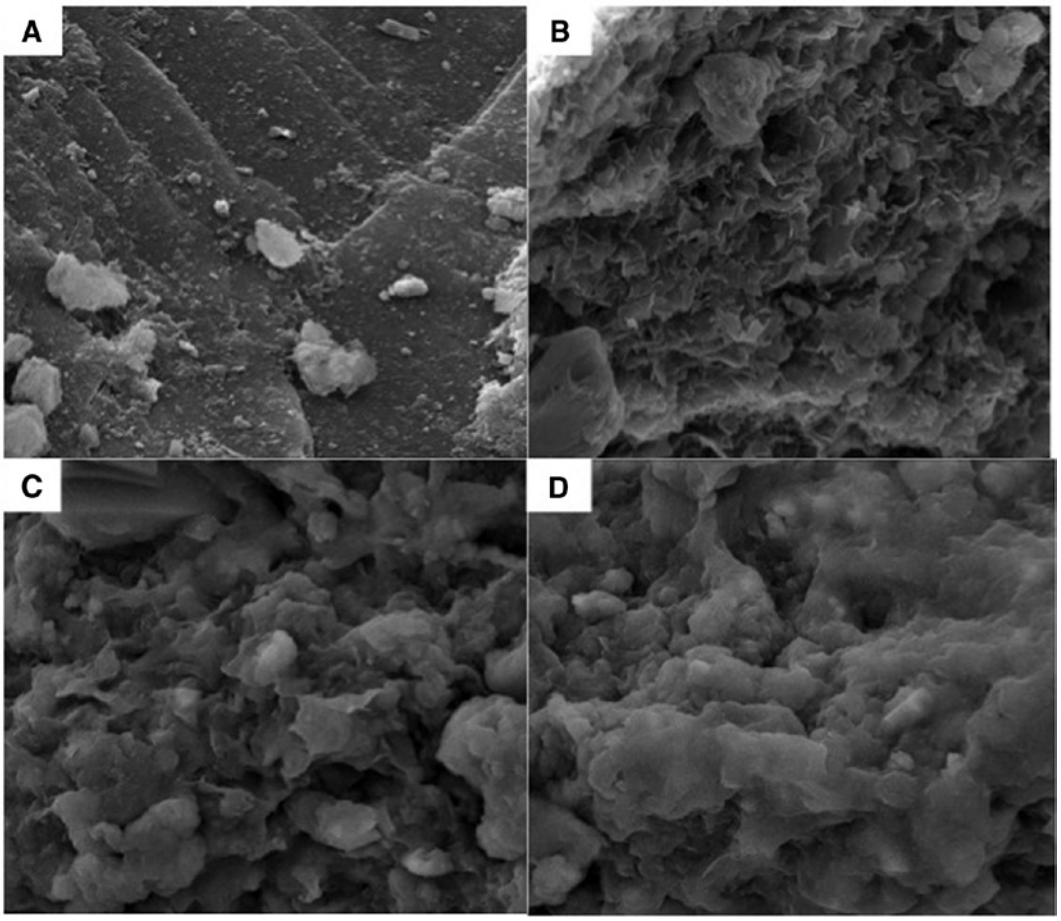

Figure 4 Surface morphology of (A) MMT, (B) OMMT (STAB), (C) OMMT (DOAB), and (D) OMMT (TOAB).

activated by STAB seemed to be made up of folded or broken layers and loose flake-like aggregate overlaid or stacked with exfoliated layers (Figure 4B). The OMMT activated by DOAB (Figure 4C) and TOAB (Figure 4D) also seemed to be made up of exfoliated layers and loose sponge-like aggregate overlaid or stacked with flocculated layers.

3.2 Pyrolysis properties

Figure 5 shows the TGA curves of MMT and OMMT. The pyrolysis was found to consist of three phases from the weight curves: phase 1, phase 2, and phase 3 (Figure 5 and Table 3). The onset and offset temperatures of each phase were different. The surface physically absorbed water (H_2Os) of MMT and OMMT was removed in phase 1. The weight loss rate curve of MMT presented a strong absorption valley. The valley temperature (T_v) and maximum pyrolysis rate (v_v) were 82°C and 0.1225 mg·min^{-1} respectively. In phase 3, the crystal lattices were broken. A water molecule was formed by two -OH and released from these crystal lattices. The structural water (-OH_2) was removed. The absorbed water (H_2Os) between MMT layers was removed in phase 2. Phase 2 of OMMT was relatively more complex than that of MMT. The intercalated LACQAS between MMT layers was pyrolyzed also in this phase. The weight loss rate curves of OMMT presented two strong absorption valleys in phase 2. The T_v and v_v were both larger than those of MMT. The longer the alkyl chain of LACQAS, the higher the pyrolysis temperature. The T_v increased as the alkyl chain lengthened. As Figure 5 and Table 3 show, the T_v was 277°C, 327°C, and 349°C at the first strong absorption valley, and 390°C, 390°C, and 405°C at the second strong absorption valley, for OMMT activated by STAB, DOAB, and TOAB, respectively. Moreover, the higher the organic content in OMMT, the more the organic content was pyrolyzed at the valley temperature in a unit time. As Figure 5 and Table 3 show, the v_v was 0.3583, 0.2854, and 0.3135 mg·min^{-1} at the first strong absorption valley, and 0.1776, 0.3911, and 0.4321 mg·min^{-1} at the second strong absorption valley, for OMMT activated by STAB, DOAB, and TOAB, respectively. It can be seen that the T_v and v_v of OMMT both increased greatly compared

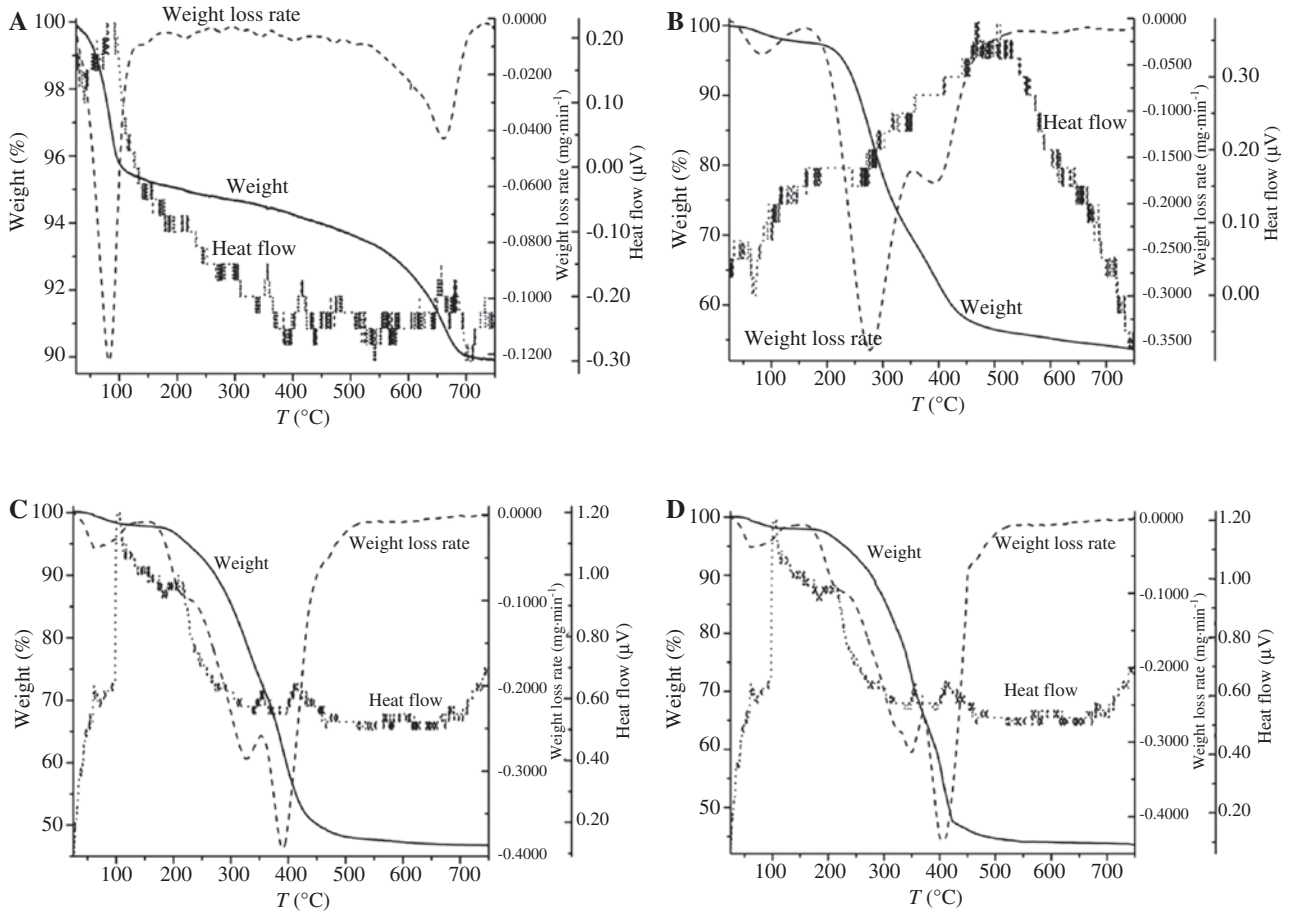

Figure 5 TGA curves of (A) MMT, (B) OMMT (STAB), (C) OMMT (DOAB), and (D) OMMT (TOAB).

with those of MMT. The *C* of MMT was 10.10% caused by the loss of absorbed and structural water in phase 1 to phase 3. The pyrolysis of OMMT mainly occurred in phase 2. The *C* was 46.37%, 53.20%, and 56.43% for OMMT activated by STAB, DOAB, and TOAB, caused by the pyrolysis of STAB, DOAB, and TOAB, respectively. The *C* coincided well with the *O* at 42.25%, 50.99%, and 54.74% of OMMT activated by STAB, DOAB, and TOAB, respectively (Table 3).

Concerning the pyrolysis kinetics of OMMT, the mechanism function is expressed by

$$G(a)=\frac{A}{\beta}\int_{T_0}^{T} e^{\frac{E_a}{RT}}\mathrm{d}T,$$

Table 3 Pyrolysis results of MMT and OMMT.

		T (°C)	T_v (°C)	v_v (mg·min⁻¹)	*C* (%)	*O* (%)	*k* (min⁻¹)
MMT	Phase 1	25–105	82	0.1225	10.1	–	–
	Phase 2	105–700	–	–			–
	Phase 3	700–750	–	–			–
OMMT (STAB)	Phase 1	25–170	–	–	46.37	42.25	–
	Phase 2	170–510	277–390	0.3583–0.1776			0.01–1.26
	Phase 3	510–750	–	–			–
OMMT (DOAB)	Phase 1	25–170	–	–	53.20	50.99	–
	Phase 2	170–520	327–390	0.2854–0.3911			0.01–0.03
	Phase 3	520–750	–	–			–
OMMT (TOAB)	Phase 1	25–170	–	–	56.43	54.74	–
	Phase 2	170–530	349–405	0.3135–0.4321			0.02–0.03
	Phase 3	530–750	–	–			–

where a is the relative thermal weight loss calculated by

$$a=\frac{m_i-m_T}{m_i-m_f},$$

where m_i is the weight at onset temperature, m_f is the weight at offset temperature, and m_T is the weight at T.

The Agrawal approximate equation is [28]

$$\int_{T_0}^{T} e^{\frac{E_a}{RT}}\mathrm{d}T=\frac{RT^2}{E_a}\left[\frac{1-2\left(\frac{RT}{E_a}\right)}{1-5\left(\frac{RT}{E_a}\right)^2}\right]e^{\frac{E_a}{RT}}.$$

Combining the above two equations, the Agrawal integral equation is written as

$$\ln\left[\frac{G(a)}{T^2}\right]=\ln\left\{\frac{AR}{\beta E_a}\left[\frac{1-2\left(\frac{RT}{E_a}\right)}{1-5\left(\frac{RT}{E_a}\right)^2}\right]\right\}-\frac{E_a}{RT}.$$

For the general reaction temperature and most E_a, the relationship among E_a, R, and T is

$$\frac{E_a}{RT}>>1;\ 1-\left(\frac{RT}{E_a}\right)\approx 1;\ 1-5\left(\frac{RT}{E_a}\right)\approx 1.$$

Thus, the Agrawal integral equation can be simplified as

$$\ln\left[\frac{G(a)}{T^2}\right]=\ln\left(\frac{AR}{\beta E_a}\right)-\frac{E_a}{RT}.$$

The relationship between $\ln\left[\frac{G(a)}{T^2}\right]$ and $\frac{1}{T}$ will be linear with a suitable $G(a)$. The E_a can be calculated from the linear slope and A from the linear intercept. In the above equations, T is the temperature, R is the universal gas constant of 8.314 J·(mol·K)$^{-1}$, β is the heating rate of 10°C·min^{-1}, E_a is the active energy, and A is the frequency factor.

According to the simplified Agrawal integral equation, T and a in phase 2 were fitted linearly using a trial-and-error method. On the basis of linearly dependent coefficients, the pyrolysis kinetics of OMMT was obtained (Table 4). In these kinetic parameters, $G(a)$ was the kinetics mechanism function used to illustrate the pyrolysis process of MMT and OMMT. The arrangement of LACQAS cations between MMT layers influenced the pyrolysis process. STAB has a long single alkyl chain, DOAB has two, and TOAB has three. STAB cations were arranged in the form of a lateral layer or a half-paraffin-type molecular structure, whereas DOAB and TOAB cations in the form of a paraffin-type molecular structure. The $G(a)$ of OMMT activated by STAB was calculated with the Avrami-Erofeev equation, $[-\ln(1-a)]^4$. Those of OMMT activated by DOAB and TOAB both were calculated with the Valensi equation, $a+(1-a)\ln(1-a)$. Their $G(a)$ were different, and so were their related linear fit equation, linearly dependent coefficient, E_a, A, and reaction order (n). The n was 4, 2, and 2 for OMMT activated by STAB, DOAB, and TOAB, respectively. E_a is the minimum required energy from a reactant molecule to an activated molecule in a chemical reaction, or the different energy between the onset and offset states of a pyrolysis process. A is a constant value determined by the reaction essence, and has nothing to do with the reaction temperature and concentration in the system. The OMMT activated by STAB, DOAB, and TOAB were pyrolyzed mainly in phase 2. Their onset and offset states were different as their E_a and A differed. As Table 4 shows, the E_a and A were 36.16 kJ·mol^{-1} and 88014.17 min^{-1} for OMMT activated by STAB, 12.67 kJ·mol^{-1} and 1.40 min^{-1} for OMMT activated by DOAB, and 13.62 kJ·mol^{-1} and 1.92 min^{-1} for OMMT activated by TOAB, respectively.

Table 4 Pyrolysis kinetics of OMMT.

	E_a (kJ·mol^{-1})	A (min^{-1})	Kinetic compensation effect equation
OMMT (STAB)	36.16	88014.17	$\ln A=0.4314E_a-4.4632$
OMMT (DOAB)	12.67	1.40	$\ln A=0.4135E_a-4.47$
OMMT (TOAB)	13.62	1.92	$\ln A=0.4103E_a-4.4428$

In the pyrolysis kinetics, the reaction rate constant (k) is always used to explain the reaction rates quantitatively. It is related to A, E_a, and T calculated by the Arrhenius equation:

$$k=Ae^{-\frac{E_a}{RT}}.$$

Table 3 presents the k of OMMT in phase 2. k is related closely to the reaction temperature, reaction medium (or solvent), catalyst, and so on, even the shape and characteristics of reactors. Therefore, during the pyrolysis processes, the k increased as the pyrolysis temperature increased. The k of OMMT activated by DOAB and TOAB were almost the same owing to their similar pyrolysis mechanisms. As Table 3 shows, the k was 0.01, 0.01, and 0.02 min^{-1} at the first strong absorption valley, and 1.26, 0.03, and 0.03 min^{-1} at the second strong absorption valley, for OMMT activated by STAB, DOAB, and TOAB, respectively.

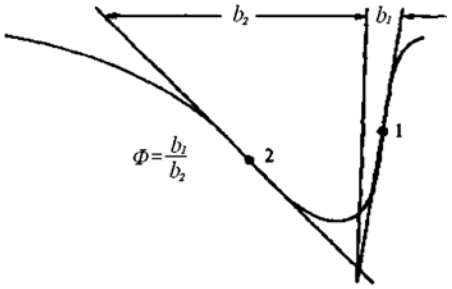

Figure 6 Φ of the DTA curve.

The kinetic compensation effect, expressing the linear relationship between ln$A$ and E_a, is a main characteristic in kinetics. It explains that A compensates for the change of E_a partly [29]:

$$\ln A = KE_a + Q,$$

where K and Q are the kinetic compensation effect parameters calculated from the linear fit between E_a and A. As Table 4 shows, the K was 0.4314, 0.4135, and 0.4103 and the Q was -4.4632, -4.47, and -4.4428 for the OMMT activated by STAB, DOAB, and TOAB, respectively. It can be seen that the pyrolysis kinetic compensation effect equations of OMMT activated by DOAB and TOAB were similar, while that of OMMT activated by STAB was not. The kinetic compensation effect parameters have nothing to do with the experimental factors; thus, the kinetic compensation effect equations can explain the pyrolysis processes of OMMT clearly, as well as their theoretical expression.

The form factor (Φ) indicates the symmetry of the heat flow curve. The symmetry will worsen as n decreases. The Φ is defined in Figure 6 [30] and only related closely to the n at $\Phi=0.63n^2$. The Φ in phase 2 was 10.08, 2.52, and 2.52 for OMMT activated by STAB, DOAB, and TOAB, respectively, showing that the OMMT activated by STAB displayed a better symmetrical heat flow curve than those of OMMT activated by DOAB and TOAB. This phenomenon coincided well with the heat flow curves collected by using TGA (Figure 5).

4 Conclusions

In this study, we prepared intercalated OMMT from pristine MMT and different LACQAS. The amount, carbon atoms, and alkyl chains of LACQAS influenced the large value of $d_{(001)}$ of OMMT significantly. The $d_{(001)}$ ranged from 1.263 nm for MMT to 2.114, 3.980, and 4.090 nm for OMMT activated by STAB, DOAB, and TOAB, respectively. The $d_{(001)}$ stabilized at 100–150 mmol·(100 g)$^{-1}$ of LACQAS/MMT. The arrangement of LACQAS cations between MMT layers was related closely to the α, L, d_0, and the configuration of the nitrogen atom in LACQAS. Single LACQAS cations arranged in the form of a lateral layer or a half-paraffin-type molecular structure between MMT layers, and dual and triple LACQAS cations in the form of a paraffin-type molecular structure. The pyrolysis temperature and maximum pyrolysis rate of OMMT increased greatly compared with those of MMT. With the help of the Agrawal integral equation, the pyrolysis kinetics of MMT and OMMT were obtained using a trial-and-error method that coincided well with the structure and pyrolysis processes.

Acknowledgments: The authors are grateful for the financial support from the National Key Technology Support Program (2012BAD24B03) and National Forestry Public Welfare Industry Research Project (210304505).

References

[1] Pagacz J, Pielichowski K. *J. Vinyl Addit. Technol.* 2009, 15, 61–76.
[2] Hosseini MG, Raghibi-Boroujeni M, Ahadzadeh I, Najjar R, Dorraji MSS. *Prog. Org. Coat.* 2009, 66, 321–327.
[3] Toth R, Voorn DJ, Handgraaf JW, Fraaije JGEM, Fermeglia M, Pricl S, Posocco P. *Macromolecules* 2009, 42, 8260–8270.
[4] Xia MS, Jiang YS, Zhao L, Li FF, Xue B, Sun MM, Liu DR, Zhang XG. *Colloid Surf. A* 2010, 356, 1–9.
[5] Naghash HJ, Mohammadrahimpanah R. *Prog. Org. Coat.* 2011, 70, 32–38.
[6] Yilmaz O, Cheaburu CN, Gulumser G, Vasile C. *Prog. Org. Coat.* 2011, 70, 52–58.
[7] Bouwe RGB, Tonle IK, Letaief S, Ngameni E, Detellier C. *Appl. Clay Sci.* 2011, 52, 258–265.
[8] Dogan H, Inan TY, Koral M, Kaya M. *Appl. Clay Sci.* 2011, 52, 285–294.
[9] Piazza D, Silveira DS, Lorandi NP, Birriel EJ, Scienza LC, Zattera AJ. *Prog. Org. Coat* 2012, 73, 42–46.
[10] Jena KK, Raju KVSN, Narayan R, Rout TK. *Prog. Org. Coat* 2012, 75, 33–37.
[11] Cui HW, Du GB. *J. Chem. Eng. Mater. Sci.* 2011, 2, 122–128.
[12] Cui HW, Du GB. *High Perform. Polym.* 2011, 23, 40–48.
[13] Cui HW, Du GB. *J Adhes. Sci. Technol.* 2011, 25, 1671–1679.
[14] Cui HW, Du GB. *Compos. Interf.* 2011, 18, 557–573.
[15] Cui HW, Du GB. *e-Polymers* 2012, 002, 1–11.
[16] Cui HW, Du GB. *Adv. Polym. Technol.* 2012, 31, 130–140.
[17] Cui HW, Du GB. *J. Compos. Mater.* 2012, 46, 2951–2958.
[18] Cui HW, Du GB. *Plast. Rubber Compos.* 2012, 4, 413–417.
[19] Cui HW, Kuo SW. *RSC Adv.* 2012, 2, 12148–12152.
[20] Cui HW, Kuo SW. *J. Polym. Res.* 2013, 20, 114.
[21] Cui HW, Kuo SW. *Polym. Bull.* 2013, 70, 3143–3153.

[22] Jordan JW. *J. Phys. Colloid Chem*. 1949, 53, 294–306.
[23] Lagaly G. *Clay Miner.* 1981, 16, 1–21.
[24] Moronta A, Ferrer V, Quero J, Arteaga G, Choren E. *Appl. Catal. A* 2001, 230, 127–135.
[25] Lagaly G, Ziesmer S. *Adv. Colloid Interf. Sci.* 2003, 100–102, 105–108.
[26] Chen DF, Wang Z, Li YK. *J. Xi'an Jiaotong U.* 2000, 34, 92–95.
[27] Tanford C. *J. Phys. Chem.* 1972, 76, 3020–3024.
[28] Agrawal RK. *J. Therm. Anal.* 1987, 32, 149–156.
[29] Hu RZ, Shi QZ. *Thermal Analysis Kinetics*. Beijing: Science Press, 2001.
[30] Kissinger HE. *Anal. Chem.* 1957, 29, 1702–1706.